Available online at www.sciencedirect.com
SCIENCE DIRECT
Journal of Catalysis 239 (2006) 431–440
JOURNAL OF CATALYSIS
www.elsevier.com/locate/jcat

Promoter and poisoning effects on NO-catalyzed dissociation on bimetallic RhCu(111) surfaces

Silvia González, Carmen Sousa, Francesc Illas *

Departament de Química Física i Centre Especial de Recerca en Química Teòrica, Universitat de Barcelona i Parc Científic de Barcelona, C/ Martí i Franquès 1, 08028 Barcelona, Spain

Received 30 November 2005; revised 14 February 2006; accepted 15 February 2006

Available online 23 March 2006

Abstract

A systematic density functional study of NO dissociation on Rh(111), Cu(111), and two different RhCu(111) bimetallic surfaces was conducted using a periodic supercell approach. Properties of the transition states, energy barriers, and transition state theory reaction rates were obtained for relevant situations involving NO adsorbed on different compositions of fcc and hcp sites. The results demonstrate that the superior activity of Rh versus Cu toward NO dissociation has its origin in the stronger adsorption on the former surface, which permits NO dissociation without the need for extra energy to the system. Moreover, the presence of Cu atoms on a Rh surface exerts a promoter effect by decreasing the energy barrier with respect to the value for the single crystal surface. In contrast, the presence of Rh atoms on a Cu surface has a poisoning effect. Analysis of the adsorption energies provides some important clues as to the modification of the corresponding energy barriers induced by the presence of the second metal. The results indicate that it is possible to improve the catalytic properties of Rh surfaces by adding small quantities of Cu, in agreement with previous experimental findings.

Keywords: NO dissociation; Bimetallic; RhCu; Rh(111); Cu(111); DFT

1. Introduction

The study of NO dissociation is technologically relevant because this is the limiting step in the reduction of NO by CO [1–23]. This is an important reaction to help control the amount of pollutants in the atmosphere, and it occurs in the three-way car exhaust catalyst [4–22]. The most active metallic catalysts toward the oxidoreduction of NO and CO are Rh, Pd, and Pt; the catalyst in actual use is a combination of these three metals. Rh is among the most active metals for NO dissociation [2,7–11,13].

The adsorption of NO on metallic surfaces has been extensively studied from an experimental and a theoretical standpoint [23–30]. Some experimental works suggest that NO adsorption on metals can be either molecular or dissociative [4,13]. For Rh, both forms are possible, depending on the temperature and coverage, with NO dissociation favored at low coverage and high temperature [4]. In the 0.25–0.50 ML coverage range, NO desorbs molecularly, with an estimated barrier of 1.17 ± 0.10 eV [7]. On Rh(111), NO dissociates at T $\sim$ 300 K, whereas lower temperatures, 170 and 160 K, are needed when the process occurs on the Rh(110) and Rh(100) surfaces, respectively. This clearly indicates that the more open Rh(110) and Rh(100) are more reactive than the more stable Rh(111) surface. A kinetic study [7] of NO dissociation monitored by temperature-programmed desorption (TPD) and spectroscopic techniques proposed values of 0.67 eV and 10^{11} s^{-1} for the activation barrier and pre-exponential factor, respectively, for NO dissociation at 0.15–0.20 ML, with NO breaking inhibited by site blocking at 400 K and a coverage of 0.50 ML. Another study based on electronic energy loss spectroscopy (EELS) reported that the activation energy was 0.83 ± 0.01 eV for NO dissociation at 0.2-ML coverage [14]. A much lower value of 0.29 eV was predicted from a spherical model catalyst using pulsed field desorption mass spectrometry (PFDMS) [31].

Numerous theoretical studies have been concerned with the active sites and reaction pathways for the mechanism of the NO

* Corresponding author.
E-mail address: francesc.illas@ub.edu (F. Illas).

0021-9517/$ – see front matter
doi:10.1016/j.jcat.2006.02.013

chemisorption and dissociation on Rh surfaces. Monte Carlo studies of the NO dissociation on Rh(100) suggested that the interaction of NO, O, and N are repulsive [28] and predicted the most favorable adsorption arrangements. In addition, a dynamic Monte Carlo model for the interaction of NO on Rh(111) can properly reproduce the TPD data, assuming interaction of NO with three-fold sites [26]. Loffreda et al. [24,25] reported periodic density functional theory (DFT) studies of the interaction of NO with Pd and Rh and concluded that on Rh(111), the most stable sites for molecular adsorption are three-fold hollows and that coadsorption of atomic N and O is favored with respect to NO in the gas phase and the clean surface. Finally, studies on the influence of the type of surface by periodic DFT models have concluded that the activation energy for NO dissociation on Rh stepped surfaces can be 1 eV lower than that on the Rh(111) surface [27].

The high activity of Rh toward NO dissociation makes this metal an ideal candidate in catalysis. In fact, it is widely used in automotive catalytic exhaust converters. However, it is very expensive, and the search for a cheaper, yet efficient catalyst for NO dissociation remains important. A reasonable proposal involves mixing Rh with other, more abundant metals in such a way to maintain the catalytic efficiency of Rh. This strategy has been used to modify the activity of other precious metals, such as Pd, using Mn [32] or Cu [33], thereby leading to bimetallic catalysts. These new types of catalysts are of interest because the presence of a second metal in a metallic catalyst modifies its reactivity and this modification can be done in a controlled manner [34–36]. Earlier research has suggested that Cu is a suitable candidate for improving the catalytic properties of Rh toward NO dissociation while simultaneously reducing the cost of producing the corresponding catalysts. This is because, under laboratory conditions, RhCu catalyst exhibits better performance than industrial Rh-containing catalysts for exhaust gas treatment in both CO oxidation and NO reduction reactions [37,38]. Moreover, Cu thin films [39] and low index surfaces [40–42] are already active toward NO dissociation, this is also the case for Cu incorporated to zeolites [43,44]. Indeed, bimetallic RhCu systems exhibit a quite peculiar reactivity [45–50]; for instance, at certain compositions, RhCu is able to adsorb more H_2 than pure Rh [45]. Recent experimental and theoretical studies have explained this behavior through a change in active sites caused by the presence of Cu [46,51], a charge transfer between the two metals [48,52], and changes in the shape of the electronic density of the bimetallic with respect to the Rh catalyst [53].

The present work reports a systematic and comparative theoretical study of the dissociation of NO on single-crystal Rh(111) and Cu(111) surfaces, as well as on two stable compositions of the same low-index surface of the RhCu alloy. These are either Rh-rich or Cu-rich and hereinafter are termed Cu@Rh(111) and Rh@Cu(111), respectively. The main aim of the present paper is to study the effect of the second metal on the NO dissociation pathway and hence provide a suitable explanation for the higher activity of the RhCu bimetallic system toward NO dissociation compared with Rh(111).

2. Experimental

2.1. Surface models

NO dissociation on Rh(111), Cu(111), and the Rh@Cu(111) and Cu@Ru(111) bimetallic surfaces has been studied using slab periodic models within the supercell approach. In all cases, the slab models were constructed using the calculated lattice parameters of 3.63 Å for Cu and 3.85 Å for Rh [30], in good agreement to the experimental values of 3.62 Å for Rh and 3.80 Å for Cu [54].

The bimetallic compositions included in the models follow from the information provided on the corresponding alloy phase diagram [55]. This indicates very low miscibility between Ru and Cu, resulting in either Rh- or Cu-rich compositions in the RhCu alloys. To model a Rh-rich composition (denoted as Cu@Rh), we started with the Rh(111) slab model and substituted one surface Rh atom by a Cu atom. The Cu-rich model (Rh@Cu) was constructed in a similar way.

Slab models consisting of three metallic layers of the monometallic and bimetallic surfaces described above were constructed. A region with a vacuum width larger than five metallic layers (>10 Å) was placed in the normal direction at the surface, to avoid interaction between the repeated slabs. The effect of the number of layers in the slab was tested for NO adsorption on Rh. Using models with three to six atomic layers led to variations in the adsorption energy of <0.1 eV, thus justifying the choice of the three-layer model. A (3×3) supercell was chosen that contains nine metal atoms per layer; thus the unit cell involved 27 metal atoms. For the bimetallic systems, this led to a composition of 1/27 or a Cu content of 2.3 wt% for the Cu@Rh and a Rh content of 5.9 wt% for the Rh@Cu. (These values are slightly larger than those corresponding to the $[4 \times 4]$ unit cell used in our previous work, where the bimetallic atomic ratio was 1/80 [30].) With respect to the supercell size, a (3×3) supercell is large enough to study NO dissociation on the various metallic and bimetallic surfaces, because the previous work using a (4×4) cell found that the influence of a second metal atom in the adsorption properties of a metallic catalyst is very small except when it is a component of the active site [30]. Nevertheless, changes due to the different composition will be analyzed in detail.

The interaction of NO, N, and O on the different surface models was studied by placing the corresponding species on just one side of the slab model. For NO adsorption, an upright geometry with the N atom pointing toward the metallic surface was considered. Following experimental and theoretical data [7,20,25,30], NO was placed above the three-fold hollow sites.

2.2. Computational details

The exploration of the potential energy surface for NO dissociation on the Cu(111), Rh(111), and RhCu(111) surfaces was carried out by periodic DFT calculations. The energy was calculated using the generalized gradient approximation (GGA), particularly through the exchange and correlation functional of Perdew and Wang (PW91) [56]. The Kresse and Joubert

[57] implementation of the projected augmented wave (PAW) method [58,59] was used to reproduce the effect of the atomic cores of the corresponding atoms in the electronic density of valence electrons. The Kohn–Sham one-electron wave functions were expanded in a basis of plane waves with kinetic energy <415 eV. The geometry optimization was carried out using a conjugate gradient algorithm. The blocked Davidson approach was used as an electronic minimization algorithm. The second-order method of Methfessel–Paxton was used to determine the partial occupancies in each Bloch function. All calculations were carried out using a $k_BT = 0.2$ eV smearing of the electron density in the corresponding electron wave function, but on convergence of the self-consistent field procedure, the total energy was extrapolated to $k_BT = 0$ eV. A $5 \times 5 \times 1$ k-points grid within the Monkhorst–Pack scheme was used to sample the Brillouin zone of the surface unit cell. A further increase on the density of k-points improves the calculated adsorption energy by 0.003 eV. Harmonic vibrational frequencies were obtained from the forces on each adsorbate nucleus in the three spatial coordinates using a finite difference scheme. The spin-restricted formalism has been used despite the fact that the isolated NO molecules have one open shell and its treatment would require spin polarization. Previous work has demonstrated that for the systems of interest in the present study, the difference between the spin-polarized and closed-shell calculations is <0.04 eV [30].

In the study of the interaction of NO, N, and O with the different surfaces, the substrate was held fixed and the coordinates of N and O atoms were fully optimized. The effect of relaxing the topmost metallic layers was been investigated for the NO adsorption on Rh(111). Using the unrelaxed surface or including the relaxation of the first or the two topmost atomic layers results in changes in the total energy of <0.2 eV. In principle, the changes in the energy likely will affect the equilibrium geometry and the transition state to a very similar extent. Calculations for NO dissociation on Rh(111) carried out without and with explicit inclusion of surface relaxation effects result in energy profiles almost parallel with energy barriers that differ by <0.10 eV. Because the conclusions of the present work are based on larger differences in the activation energies, using the energy profiles derived from calculations that neglect surface relaxation effects is perfectly justified. Note also that such a small reduction in the energy barriers will also appear for NO on the other surfaces, making the relative difference between the relevant barriers calculated for the relaxed surfaces even smaller.

All calculations were carried out using the Vienna Ab-initio Simulation Package (VASP) computational code [60,61]. The minimum reaction path was calculated using the climbing image nudged elastic band (NEB) method [62] and dimer method techniques [63], both as implemented in the VASP package. The latter was used to refine the transition state structure when necessary. The activation energy barrier for breaking NO was obtained from the difference between the energy of the transition state for the NO dissociation and the energy of the molecular adsorbed state. For those cases where NO dissociation is likely to be the most favored process, the reaction rate constant for NO dissociation from the adsorbed state was estimated from transition state theory, using the vibrational frequencies in the harmonic approach to estimate the entropy contribution to the free energy variation [64]. Hence,

$$k_{NO} = \left(\frac{k_B T}{h}\right)\left(\frac{q_{TS}}{q_{NO}}\right) e^{(-E_{act}/k_B T)}, \quad (1)$$

where k_{NO} is the reaction rate constant; k_B is the Boltzman constant; T is the temperature (300 K in this case); q_{TS} and q_{NO} are the vibrational partition functions of the transition state and NO equilibrium geometry, respectively; h is the Planck constant; and E_{act} is the activation energy for NO dissociation corrected for the zero point energy.

3. Results and discussion

The NO dissociation reaction on the different metallic and bimetallic surfaces was studied assuming that the incoming molecule adsorbs at a given site of the surface (either fcc or hcp three-fold hollow sites) and then dissociates in a single step through the corresponding transition state structure. The energy, geometry, and vibrational frequencies were calculated for the reactants, transition state, and final products. The geometry and vibrational frequencies of reactants have been reported previously [30], the transition state structures were located by the NEB algorithm and characterized by proper frequency analysis, and the products correspond to the N and O atoms coadsorbed, each atom on a three-fold hollow site. Along the reaction pathway, the energy of both fragments (NO and surface model) at infinite distance was been taken as the reference energy. This reference is the sum of energy of the molecule (E_{NO}) in vacuum and the clean surface (E_{Rh}, E_{Cu}, $E_{Rh@Cu}$, or $E_{Cu@Rh}$).

In this paper, the results for products and reactants adsorption are presented first, followed by a discussion of the reaction pathways for NO dissociation on the fcc and hcp three-fold hollow sites of the metallic single-crystal Rh(111) and Cu(111) and on the same sites of the bimetallic Cu@Rh and Rh@Cu(111) surfaces. In the latter cases, different sites are considered as a function of the site composition.

3.1. N and O atomic adsorption on Rh, Cu, Rh@Cu, and Cu@Rh models

The final products of NO dissociation involve the coadsorption of the N and O separated atoms. Tables 1 and 2 report the adsorption energies and the geometry of both atoms adsorbed on fcc and hcp sites of the different models, respectively. The present results compare well with available experimental data for the adsorption of O and N atoms on Rh [65–69] and Cu [70] surfaces. The obtained result for coadsorption energy and geometry are very similar in both sites. The coadsorption energy is obtained by assuming that the adsorbed atoms are close to one another in contiguous fcc or hcp sites. For the bimetallic surfaces, there are two possibilities, depending on whether N or O is located at a mono-metallic or a bimetallic site. The trend in the coadsorption energy with respect the bimetallic composition site is that it increases (in absolute value) with the number

Table 1
Calculated properties for N and O adsorption on the fcc site of Rh(111), Cu(111) and of the Cu@Rh(111) and Rh@Cu(111) bimetallic surfaces. Adsorption energies are in eV and distances in Å. The co-adsorption energy corresponds to a situation with the N and O atoms sitting in contiguous fcc sites

Surface	Composition site		E_{coads}	$d_{N–Rh}$	$d_{O–Rh}$	$d_{N–Cu}$	$d_{O–Cu}$
	N	O					
Rh	Rh	Rh	−2.86	1.890 (1.87 [68])	2.014 (2.00 [66])		
Cu@Rh	Rh	RhCuRh	−2.76	1.894	1.907		2.034
	RhCuRh	Rh	−2.62	1.856	1.999	1.921	
Cu	Cu	Cu	−0.52			1.823 (1.89 [70])	1.846
Rh@Cu	Cu	CuRhCu	−0.79		1.906	1.794	1.930
	CuRhCu	Cu	−1.44	1.804		1.889	1.883

Table 2
Calculated properties for N and O adsorption on the hcp site of Rh(111), Cu(111) and of the Cu@Rh(111) and Rh@Cu(111) bimetallic surfaces. Adsorption energies are in eV and distances in Å. The co-adsorption energy corresponds to a situation with the N and O atoms sitting in contiguous hcp sites

Surface	Composition site		E_{coads}	$d_{N–Rh}$	$d_{O–Rh}$	$d_{N–Cu}$	$d_{O–Cu}$
	N	O					
Rh	Rh	Rh	−2.98	1.889 (1.87 [68])	1.994 (2.00 [66])		
Cu@Rh	Rh	RhCuRh	−2.82	1.879	1.937		2.053
	RhCuRh	Rh	−2.56	1.854	1.977	1.944	
Cu	Cu	Cu	−0.04			1.826 (1.89 [70])	1.845
Rh@Cu	Cu	CuRhCu	−0.32		2.012	1.802	1.918
	CuRhCu	Cu	−0.99	1.800		1.893	1.865

of Rh atoms in the site, as would be expected from the higher affinity of Rh for both N and O. The distance from the N or O atoms to the surface metal atoms also follows this trend. In all cases, the N–Rh and O–Rh distances are shorter than the N–Cu and O–Cu distances

3.2. NO adsorption on Rh, Cu, Rh@Cu, and Cu@Rh models

The molecular NO adsorption on Rh, Cu, and bimetallic surfaces were calculated using the (3 × 3) cell described in Section 2.1. The molecule was adsorbed on hcp and fcc sites. The calculated properties, adsorption energy (E_{ads}), geometry, and molecular vibration frequency of adsorbed NO (ν_{NO}) are summarized in Tables 3 and 4 for the fcc and hcp sites, respectively, to facilitate analysis of the changes induced by composition. First, note that all calculated values are very similar to those obtained previously for a large (4 × 4) unit cell [30]. Because the adsorption properties of these surfaces with respect to NO have been discussed at length in previous work, here we highlight only the trends relevant to the NO dissociation process. (A more detailed description is provided elsewhere [30].) The calculated adsorption properties compare well with the existing experimental values. The properties presented in Tables 3 and 4 indicate that, in agreement with previous experimental and theoretical values, NO adsorption on Cu is weaker than on Rh atoms, by 1.37 eV for the fcc site and 1.74 eV for the hcp site. In contrast, the geometric parameters and vibrational frequencies are very similar on both surfaces.

For the Cu@Rh system, the adsorption properties of NO on purely Rh sites of this bimetallic system are similar to those on Rh surface, as would be expected based on the local character of the interaction and show that ensemble effects caused by the presence of Cu (creation of new sites) dominate electronic effects (modification of the metal band structure). The NO adsorption energies are −2.34 and −2.50 eV on the fcc and hcp Rh sites Cu@Rh(111) (Tables 3 and 4), compared with −2.49 and −2.62 eV for the same sites of Rh(111). Therefore, the adsorption energy difference on pure Rh sites due to alloying is of 0.15 for the fcc site and 0.12 eV for the hcp site. Moreover, differences in geometry are negligible. The presence of a Cu atom in the active site induces significant changes in NO adsorption energy, which become −2.26 and −2.31 for the bimetallic RhCuRh fcc and hcp sites, respectively. Then alloying results in corresponding decreases in NO absorption energy of 0.23 and 0.31 eV. These changes are slightly greater than those found for a (4 × 4) unit cell [30] and reflect an effect of the bimetallic composition. In all cases, the equilibrium geometry of the adsorbed molecule on Rh or RhCuRh sites is noticeably different and, in the bimetallic sites, with a marked trend of NO to sit closer to Rh atoms. Another interesting result of this work concerns the much greater tilting of adsorbed NO on Cu@Rh bimetallic sites. Using a combination of TPD and HREELS techniques, a lying-down NO configuration was detected for NO on Rh(100) and Rh(110) [8,9,11,19]. This species has been identified as a precursor for NO disso-

Table 3
Adsorption properties for NO on the fcc site of Rh(111), Cu(111) and the Cu@Rh(111) and of the Rh@Cu(111) bimetallic surfaces. Adsorption energies are in eV, distances in Å and the vibrational frequencies in cm^{-1}. The tilting angle θ is in degrees and is the angle formed by the molecular bond and one normal line to the surface

Surface	Composition site	E_{ads}	d_{N-O}	d_{N-Rh}	d_{N-Cu}	θ	ν_{NO}
Rh	Rh	−2.49	1.217	2.059		0	1544
		(−1.48 [20])	(1.15 [22])	(2.17 [22])			(1515 [22])
Cu@Rh	Rh	−2.34	1.217	2.056		1	1539
	RhCuRh	−2.26	1.209	1.956	2.227	13	1600
Cu	Cu	−1.12	1.220		2.005	2	1501
Rh@Cu	Cu	−1.25	1.217		1.981	5	1517
	CuRhCu	−1.93	1.211	1.931	2.085	1	1567

Table 4
Adsorption properties for NO on the hcp site of Rh(111), Cu(111) and of the Cu@Rh(111) and Rh@Cu(111) bimetallic surfaces. Adsorption energies are in eV, distances in Å and the vibrational frequencies in cm^{-1}. The tilting angle θ is in degrees and is the angle formed by the molecular bond and one normal line to the surface

Surface	Composition site	E_{ads}	d_{N-O}	d_{N-Rh}	d_{N-Cu}	θ	ν_{NO}
Rh	Rh	−2.62	1.218	2.047		0	1523
		(−1.48 [20])	(1.15 [22])	(2.17 [22])			(1515 [22])
Cu@Rh	Rh	−2.50	1.220	2.046		1	1519
	RhCuRh	−2.31	1.213	1.980	2.493	14	1590
Cu	Cu	−0.88	1.217		2.023	0	1519
Rh@Cu	Cu	−1.00	1.212		1.993	4	1519
	CuRhCu	−1.69	1.209	1.934	2.099	5	1572

ciation on these surfaces. In contrast, there is no evidence of a stable tilted species on Rh(111) [19] surfaces. Nonetheless, it is worth mentioning that earlier experimental and theoretical studies of NO dissociation on Rh(111) [7], Rh(110) [23], and Rh(100) [32] suggested the existence of a precursor state to NO dissociation with the N–O bond parallel to the surface. The more tilted structure of NO on the Cu@Rh bimetallic sites seems to indicate that the presence of Cu in the active site favors this precursor state. This is analyzed in detail in the forthcoming discussion. Indeed, this may be a possible explanation of the better activity of the RhCu bimetallic catalyst with respect to Rh observed experimentally [37].

The adsorption properties of NO adsorbed on Cu-only sites of the Rh@Cu system are also very similar to the properties of NO adsorption on Cu(111), with differences in adsorption energy of 0.13 for the fcc site and 0.12 eV for the hcp site and with negligible changes in geometry. In contrast to Cu@Rh, however, the presence of Rh atoms slightly stabilizes NO adsorption. Later, we show that this has a decisive influence on the NO dissociation process. The presence of Rh induces a considerable difference in adsorption on bimetallic sites. NO adsorption is enhanced with respect to Cu-only sites, and the molecule prefers to sit closer (by ∼0.15 Å) to the Rh atom in a configuration reminiscent of a Rh–Cu bridge site.

3.3. NO dissociation on Rh(111) and Cu (111) single-crystal surfaces

For NO dissociation on (fcc and hcp) three-fold hollow sites of Rh(111), the zero-point-corrected energy barriers are almost the same, 1.53 and 1.59 eV, respectively (Tables 5 and 6).

Table 5
Calculated properties for the NO dissociation transition state on fcc sites of the Rh(111), Cu(111) and of the Cu@Rh(111) and the Rh@Cu(111) bimetallic surfaces. The calculated activation energy (E_{act}) corrected by zero point of energy is reported in eV, the distances in Å, and the imaginary molecular vibrational frequencies (ν_{imag}) in cm^{-1}. Transition state theory reaction rate constants in s^{-1} are given for those cases where NO dissociation is favored over desorption or recombination

Surface	Composition site	E_{ads}	d_{N-O}	d_{N-Rh}	d_{N-Cu}	ν_{imag}	k_{NO}
Rh	Rh	1.53 (0.83 [14])	1.733	1.888		502	5×10^{-13}
Cu@Rh	Rh	1.29	1.733	1.888		482	5×10^{-9}
	RhCuRh	1.21	1.733	1.888	2.570	480	1×10^{-7}
Cu	Cu	1.58	1.638		1.790		
Rh@Cu	Cu	1.74	1.638		1.790		
	CuRhCu	1.68	1.722	1.867	2.033		

Both values are obtained by properly taking into account the zero-point vibrational energy. This correction represents an almost constant decrease of the uncorrected barriers by ∼0.03–0.04 eV, only. Fig. 1 shows the calculated minimum reaction pathway and indicates that NO dissociation is thermodynamically favored with respect to molecular adsorption or desorption. The computed barrier is larger than the one predicted experimentally (0.86 eV) [14], but similar to that reported by Loffreda et al. [27] (1.61 eV) using a similar approach. In any case, the large barrier predicted by the calculations is in agreement with the low activity of Rh(111) toward NO dissociation. To decrease this barrier, Loffreda et al. suggested including defects in the surface. The presence of defects can also be the

Table 6
Calculated properties for the NO dissociation transition state on hcp sites of the Rh(111), Cu(111) and of the Cu@Rh(111) and the Rh@Cu(111) bimetallic surfaces. The calculated activation energy (E_{act}) corrected by zero point of energy is reported in eV, the distances in Å, and the imaginary molecular vibrational frequencies (ν_{imag}) in cm^{-1}. Transition state theory reaction rate constants in s^{-1} are given for those cases where NO dissociation is favored over desorption or recombination

Surface	Composition site	E_{ads}	d_{N-O}	d_{N-Rh}	d_{N-Cu}	ν_{imag}	k_{NO}
Rh	Rh	1.59	1.705	1.884		531	5×10^{-14}
Cu@Rh	Rh	1.38	1.705	1.884		518	1×10^{-10}
	RhCuRh	1.24	1.705	1.884	2.420	488	5×10^{-8}
Cu	Cu	1.47	1.612		1.811		
Rh@Cu	Cu	1.76	1.786		1.885		
	CuRhCu	1.98	1.796	1.852	1.904		

reason for the difference between the calculated and experimental activation energy. In this work, we focus on the effect of a second metal on the activation energy.

Fig. 2 reports the minimum energy path for NO dissociation on the three-fold hollow sites of the Cu(111) surface. NO adsorption is less favored on Cu(111) than on the corresponding Rh surface; the fcc site is more stable than the hcp site by 0.24 eV. The energy barrier for NO dissociation is again similar for both the fcc and hcp sites, ∼1.5 eV. This is along the same order as the energy barriers predicted for NO dissociation on Rh(111). Hence these results indicate that the dissociation is more favored on the Rh surface than on the Cu surface, not due to a lower barrier from the adsorbed state, but rather because in the reaction pathway, which on Rh(111) is thermodynamically favored, the transition state lies below the reference energy. In other words, on Rh(111) the adsorption energy is sufficient to enable NO dissociation without supplying extra energy to the system NO, whereas on Cu(111) it is not. This finding is in agreement with the mechanism proposed in the literature, in which molecular adsorption is an essential step. Note also that on Cu(111), NO desorption will occur before the energy barrier for NO dissociation can be surmounted.

3.4. NO dissociation on Cu@Rh(111) and Rh@Cu(111) bimetallic surfaces

To study NO dissociation on the RhCu bimetallic surfaces, four possibilities must be considered for this reaction depending on the composition of the bimetallic site. For instance, for the Cu@Rh(111) surface, it is necessary to consider the active site formed by Rh atoms only or the one including a single Cu atom. Each possibility has been studied for both three-fold hollow sites. Similarly, four possibilities must be considered for the reactivity of the Rh@Cu system.

The reaction pathways for NO dissociation on Cu@Rh are shown in Fig. 3. This figure includes the relative energy with respect to gas-phase NO plus the corresponding surface model, the transition state, and separated adsorbed N and O atoms. The differences in the geometry of the transition states in Rh and Cu@Rh systems for these sites are negligible (Tables 5 and 6). The only remarkable result concerns the differences between the distances of reacting atoms and the metal surface (Fig. 4). In all cases, the N–Cu distance is longer than the N–Rh value, as would be expected from the stronger preference of N and O to bind to Rh rather than to Cu.

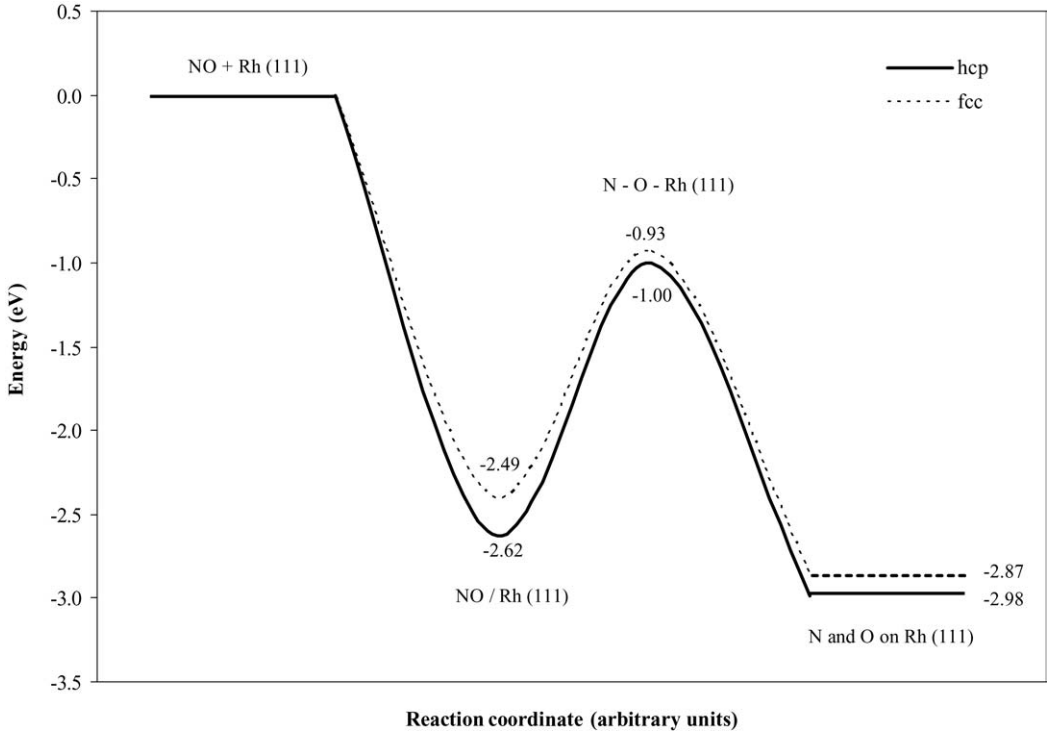

Fig. 1. Calculated minimum reaction pathway of NO dissociation on three-fold hollow sites of the Rh(111) surface.

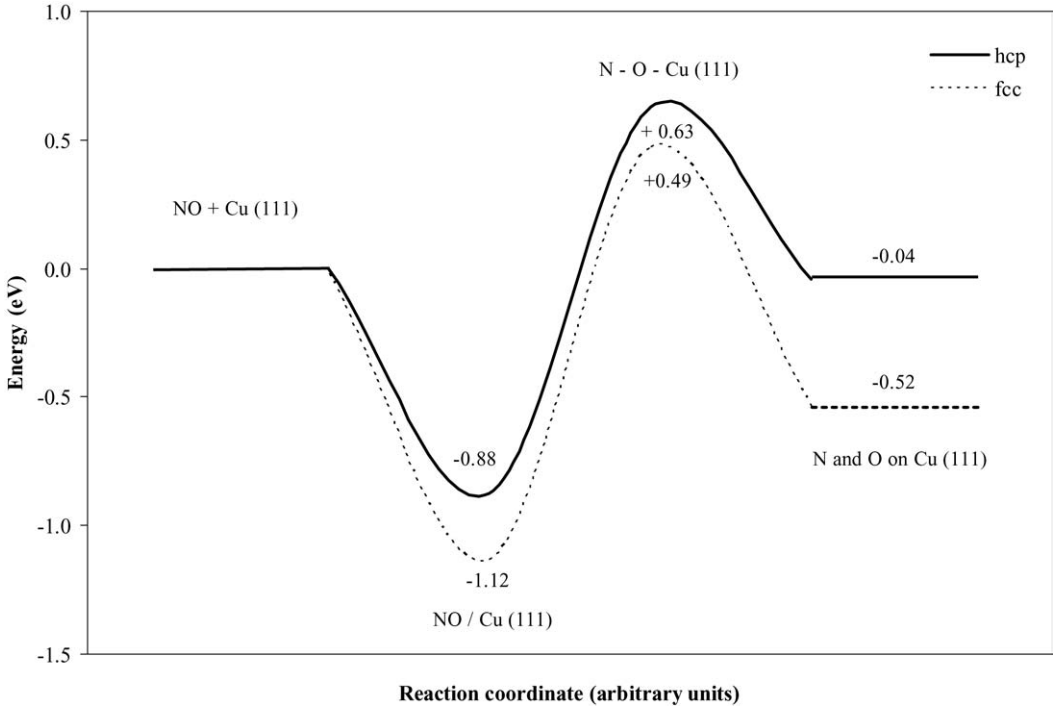

Fig. 2. Calculated minimum reaction pathway of NO dissociation on three-fold hollow sites of the Cu(111) surface.

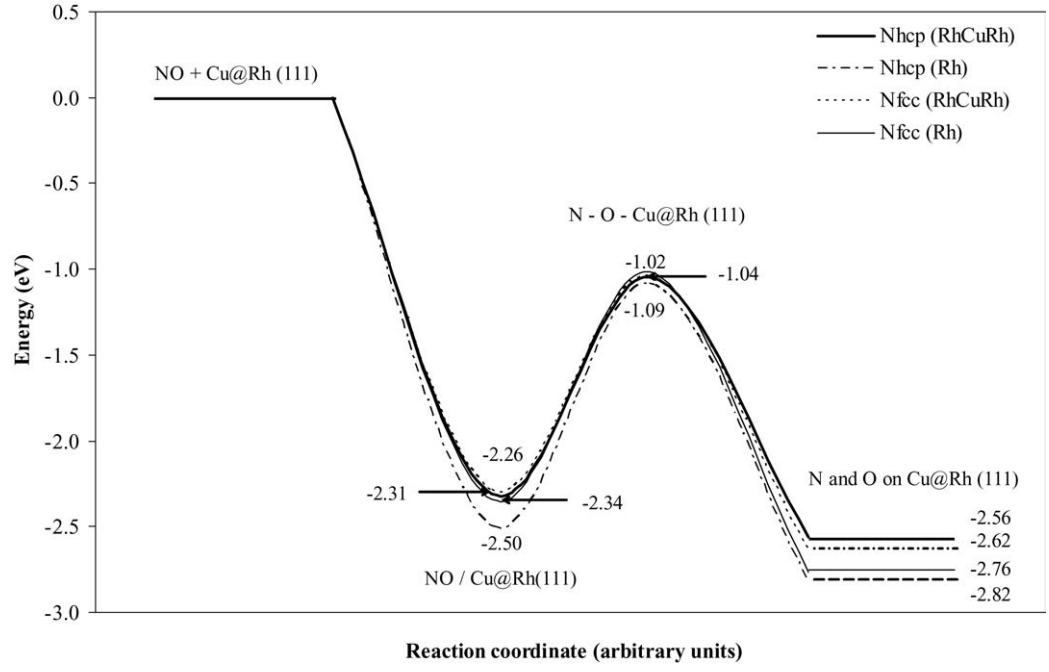

Fig. 3. Calculated minimum reaction pathway of NO dissociation on Rh and RhCu bimetallic sites of the Cu@Rh(111) surface.

An interesting result is that the transition-state energies for NO dissociation above a pure Rh fcc site of Cu@Rh and above a bimetallic Rh–Cu–Rh fcc site, relative to the separated systems, are practically the same (Fig. 3), with a difference of only 0.08 eV. A slightly larger difference (0.14 eV) is found for the corresponding hcp sites. Hence, it can be concluded that, at variance with adsorption properties that are dominated by the composition of the active site, the NO transition-state energy depends on the overall surface compositions being almost equal for different sites of a given bimetallic surface. The resulting energy barrier for NO dissociation on pure Rh sites of Cu@Rh(111) is reduced considerably (by 0.24 eV) with respect to the corresponding barrier for the single-crystal Rh(111) surface. But a large part of this difference already arises from the slightly destabilizing effect of adsorbed NO caused by the nearby presence of Cu. In this sense, adsorption energy variations induced by the change of the bimetallic composition can provide valuable information about its catalytic activity.

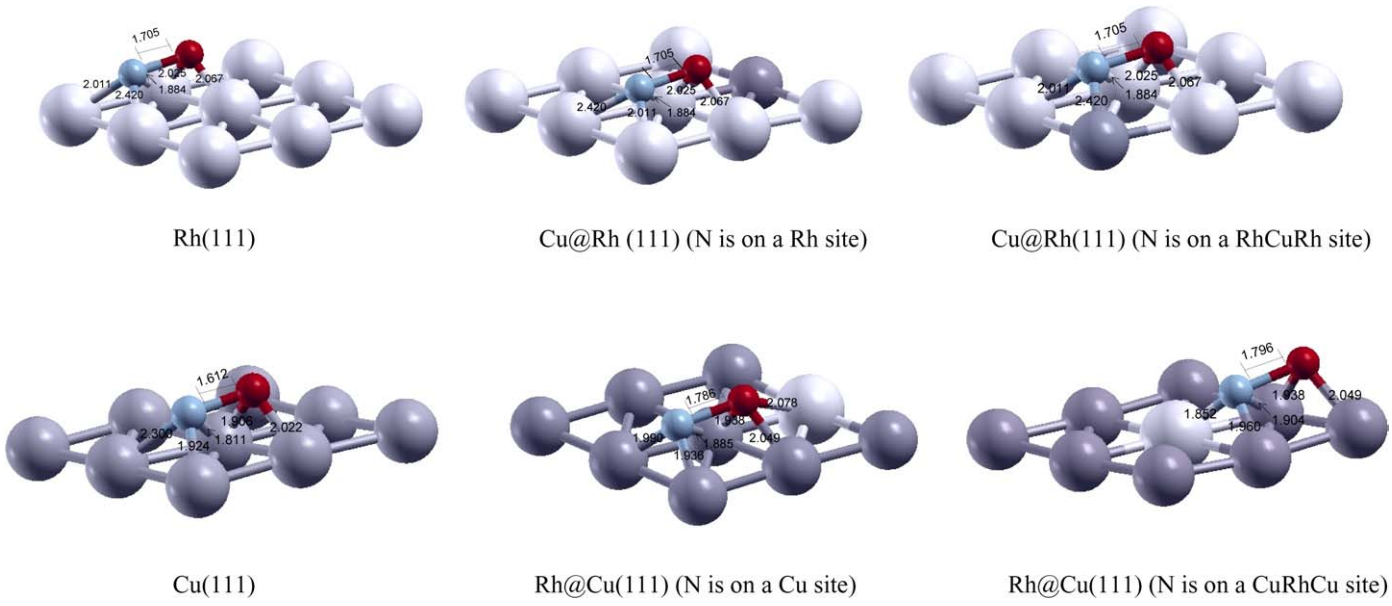

Fig. 4. Schematic representation of relevant transition state geometries for NO dissociation on hcp sites. Large light-grey spheres correspond to Rh atoms, large dark-grey to Cu, small dark-grey (red in web version) to O and small light-grey (blue in web version) to N atoms. All distances are in Å.

The calculated transition state theory rate constants (k_{NO}) at 300 K are four orders of magnitude larger for the same site of the bimetallic system. An analysis of the different contributing terms to the rate constant shows that the difference arises from the different energy barriers; prefactors for dissociation at these two surfaces are almost the same. The NO dissociation rate constant is increased by two orders of magnitude when NO dissociation occurs on a bimetallic site, despite the presence of an energy barrier almost the same as that for the pure Rh site. The foregoing results lead us to a theoretical explanation of the reported experimental data [37,38], which indicate that Cu acts like promoter of the catalytic activity of Rh surface toward NO and CO oxidation. Although obviously the NO dissociation will be more likely in Rh sites than in bimetallic sites, it is interesting to include both cases for comparison. On the other hand, NO can be dissociated on RhCu sites if all Rh sites are occupied.

The reaction pathways for NO dissociation on Rh@Cu(111) are displayed in Fig. 5. As in the Cu@Rh(111) bimetallic surface discussed above, four possible reaction paths are explored depending on the site geometry (fcc or hcp) and composition (Cu or Cu–Rh–Cu sites). Contrary to what occurs for the Cu@Rh(111) case, the pathways for each composition of Rh@Cu(111) are very different even though the activation energies of NO on both Cu-only three-fold sites are very similar; with the difference in energy profiles resulting from the ∼0.25 eV difference in adsorption energy. In contrast, for the hcp bimetallic site, the NO dissociation barrier is ∼0.30 eV higher than that corresponding to the fcc site. To understand this difference, it is necessary to analyze the geometry of both transition states. For the hcp site, the closer that N is to Cu, the more the reaction is impeded (see Tables 5 and 6).

To analyze the effect of the presence of one Rh atom on the Cu surface, we compare the energy barriers to those corresponding to the Cu(111) surface. In contrast to what is found for the Cu@Rh system, here it appears that the presence of Rh atoms on the Cu surface does not favor NO dissociation. On the contrary, the energy barriers for the bimetallic surface are all higher than those for the Cu(111) surface, by 0.10 eV for the fcc site and 0.50 eV for hcp site, due in part to the fact that the presence of Rh atoms enhances NO adsorption. Note again that, as for the Cu(111) surface, NO desorption is preferable to dissociation except for the RhCuRh fcc bimetallic site, for which the reverse reaction is more favorable than dissociation.

4. Conclusion

This paper reports a systematic study of the NO dissociation reaction at fcc and hcp sites of the Rh(111) and Cu(111) single-crystal metal surfaces and with the same geometric arrangement and two different bimetallic RhCu compositions, one Rh-rich and the other Cu-rich. The principal aim of this work is to study the changes in reactivity induced by the presence of the second metal. Toward this end, minimum energy pathways and transition states were located for 12 different situations involving different sites and different site compositions.

Analysis of the energy profiles for NO dissociation on the Rh(111) and Cu(111) single crystal surfaces shows that the superior activity of Rh toward this reaction is due to the fact that in this case, the complete reaction path occurs below the energy of the separate reactants. Hence, the NO adsorption energy is sufficient to overcome the subsequent energy barrier. This is not the case for NO dissociation on the Cu(111) surface, where desorption is more favorable.

The results reported herein indicate that a single Cu atom is sufficient to affect the catalytic properties of Rh. In part, this effect arises from a change in NO adsorption energy, which leads to a concomitant decrease in the NO dissociation energy barrier. Hence, the presence of Cu at the Rh(111) surface promotes NO dissociation. The origin of this catalytic effect is kinetic but can be anticipated from the study of NO adsorption energy, which

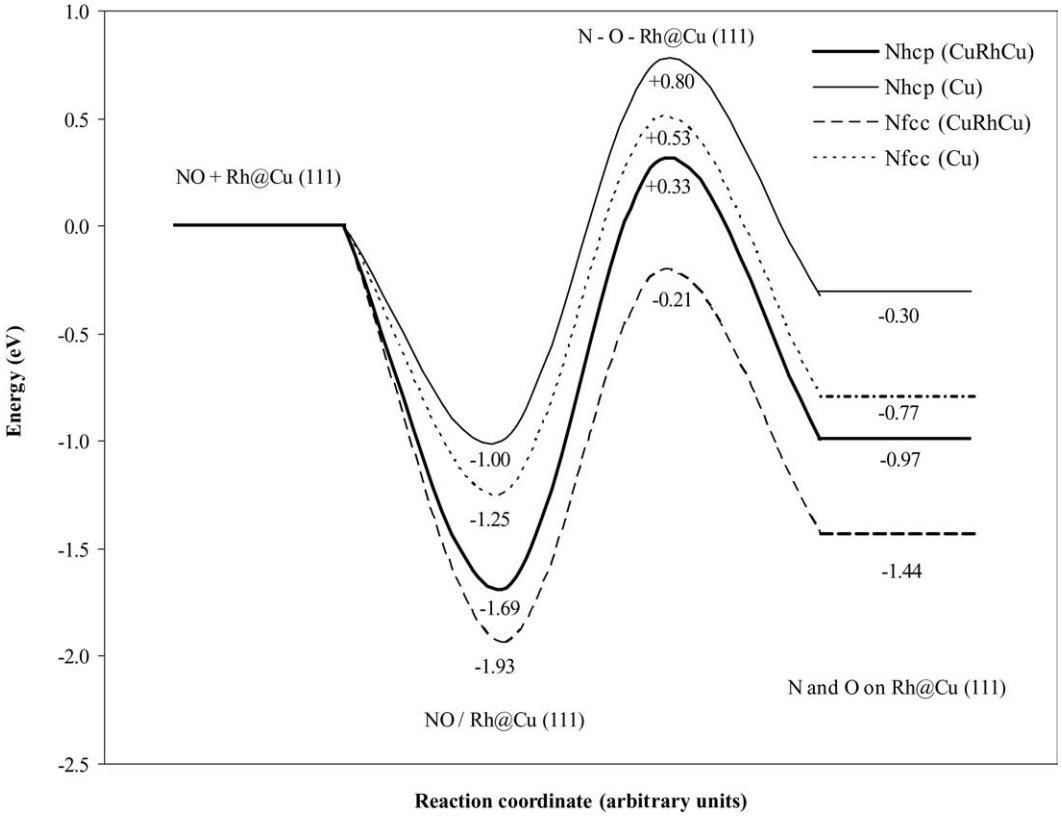

Fig. 5. Calculated minimum reaction pathway of NO dissociation on Cu and RhCu bimetallic sites of the Rh@Cu(111) surface.

indeed depends on the alloy composition. Moreover, analysis of the adsorbed NO geometry provides some additional clues. In fact, the existence of a tilted configuration for NO on the bimetallic sites of the Cu@Rh(111) system, which is similar to a promoter state found experimentally in Rh(100) and Rh(110) but not detected in Rh(111), can also explain the further decrease in the NO dissociation barrier. On the other hand, the presence of Rh atoms on Cu(111) has a totally different effect; it poisons the surface by increasing the NO energy dissociation barrier with respect to Cu(111). Again, part of this effect arises from the extra stabilization of the adsorbed molecule caused by the presence of Rh.

To conclude, the presence of Cu atoms in Rh(111) enhances the reactivity of Rh(111) toward NO dissociation, whereas the presence of Rh atoms in Cu(111) decreases the reactivity of Cu(111). The origin of this kinetic difference can be deduced in part from the changes in adsorption energy. Finally, it is important to note that the promoter effect of Cu to dissociate NO on Rh(111) is similar to recent findings reported by Mavrikakis et al. [71] for the dissociation of O_2 on $Pt_3Co(111)$. These authors found that the presence of a small quantity of Co on Pt(111) largely facilitates O–O bond breaking. Further work is needed to develop and validate simple rules that will enable the design of efficient bimetallic catalysts for a given reaction.

Acknowledgments

The authors thank D. Torres for helping with the NEB and rate constant calculations. S.G. thanks the Universitat de Barcelona for supporting her predoctoral research. Financial support was provided by the Spanish Ministry of Education and Science (projects CTQ2005-08459-CO2-01 and UNBA05-33-001) and Generalitat de Catalunya (projects 2005SGR-00697 and 2005 PEIR 0051/69 and Distinció per a la Promoció de la Recerca Universitària de la Generalitat de Catalunya, to F.I.). Computer time was provided by the Centre de Supercomputació de Catalunya, CESCA, Centre Europeu de Parallelisme de Barcelona, CEPBA, and CEBPA-IBM-Research Institute, CIRI, through generous grants from Universitat de Barcelona, Fundació Catalana per a la Recerca, and CIRI.

References

[1] P. Granger, J.J. Lecomte, L. Leclercq, G. Leclercq, Appl. Catal. A 208 (2001) 369.
[2] G. Comelli, V.R. Dhanak, M. Kiskinova, K.C. Prince, R. Rosei, Surf. Sci. Rep. 32 (1998) 165.
[3] F. Zaera, C.S. Gopinath, J. Mol. Catal. A 167 (2001) 23.
[4] W.A. Brown, D.A. King, J. Phys. Chem. B 104 (2000) 2578.
[5] G. Ertl, H. Knözinger, J. Weitkamp, Handbook of Heterogeneous Catalysis, vols. 3–5, Wiley–VCH, Munich, 1997.
[6] K.C. Taylor, Automobile Catalytic Converters, in: J.R. Anderson, M. Boudart (Eds.), Catalysis Science and Technology, Springer, Berlin, 1984.
[7] H.J. Borg, J.F.C.J.M. Reijerse, R.A. van Santen, J.W. Niemantsverdriet, J. Chem. Phys. 101 (1994) 10052.
[8] J.S. Villarubia, W. Ho, J. Chem. Phys. 87 (1987) 750.
[9] P. Ho, J.M. White, Surf. Sci. 137 (1984) 103.
[10] T.W. Root, L.D. Schmidt, G.B. Fisher, Surf. Sci. 150 (1985) 173.
[11] T.W. Root, L.D. Schmidt, G.B. Fisher, Surf. Sci. 134 (1983) 30.

[12] S. Lizzit, A. Baraldi, D. Cocco, G. Comelli, G. Paolucci, R. Rosei, M. Kiskinova, Surf. Sci. 410 (1998) 228.
[13] F. Garin, Appl. Catal. A 222 (2001) 183.
[14] T.W. Root, G.B. Fisher, L.D. Schmidt, J. Chem. Phys. 85 (1986) 4679.
[15] C.H.F. Peden, D.N. Belton, S.J. Schimieg, J. Catal. 155 (1995) 204.
[16] F. Zaera, C.S. Gopinath, Phys. Chem. Chem. Phys. 5 (2003) 646.
[17] F. Zaera, C.S. Gopinath, J. Chem. Phys. 111 (1999) 8088.
[18] T. Saito, M. Imamura, N. Matsubayashi, K. Furuya, T. Kikuchi, H. Shimada, J. Electron Spectrosc. Relat. Phenom. 119 (2001) 95.
[19] G. Cautero, C. Astaldi, P. Rudolf, M. Kiskinova, R. Roseib, Surf. Sci. 258 (1991) 44.
[20] V.P. Zhdanov, B. Kasemo, Catal. Lett. 40 (1996) 197.
[21] K.B. Rider, K.S. Hwang, M. Salmeron, G.A. Somorjai, J. Am. Chem. Soc. 124 (2002) 5588.
[22] Y.J. Kim, S. Thevuthasan, G.S. Herman, C.H.F. Peden, S.A. Chambers, D.N. Belton, H. Permana, Surf. Sci. 359 (1996) 269.
[23] D. Liao, K.M. Glassford, R. Ramprasad, J.B. Adams, Surf. Sci. 415 (1998) 11.
[24] D. Loffreda, D. Simon, P. Sautet, J. Chem. Phys. 108 (1998) 6447.
[25] D. Loffreda, D. Simon, P. Sautet, Chem. Phys. Lett. 291 (1998) 15.
[26] C.G.M. Hermse, F. Frechard, A.P. van Bavel, J.J. Lukkien, J.W. Niemantsverdriet, R.A. van Santen, A.P.J. Jansen, J. Chem. Phys. 118 (2003) 7081.
[27] D. Loffreda, D. Simon, P. Sautet, J. Catal. 213 (2003) 211.
[28] A.P. van Bavel, C.G.M. Hermse, M.J.P. Hopstaken, A.P.J. Jansen, J.J. Lukkien, P.A.J. Hilbers, J.W. Niemantsverdriet, Phys. Chem. Chem. Phys. 6 (2004) 1830.
[29] L.A. Avalos, V. Bustos, R. Uñac, F. Zaera, G. Zgrablich, J. Mol. Catal. A 228 (2005) 89.
[30] S. González, C. Sousa, F. Illas, J. Phys. Chem. B 109 (2005) 4654.
[31] N.J. Kruse, Mol. Catal. A 163 (2000) 79.
[32] D. Loffreda, F. Delbecq, D. Simon, P. Sautet, J. Chem. Phys. 115 (2001) 8101.
[33] N. Lopez, J.K. Norskov, Surf. Sci. 477 (2001) 59.
[34] J.A. Rodriguez, Surf. Sci. Rep. 24 (1996) 223.
[35] J.H. Sinfelt, Bimetallic Catalyst, Wiley, New York, 1983.
[36] V. Ponec, Appl. Catal. A 222 (2001) 31.
[37] L. Petrov, J. Soria, L. Dimitrov, R. Cataluña, L. Spasov, P. Dimitrov, Appl. Catal. B 8 (1996) 9.
[38] X. Courtois, V. Perichon, Appl. Catal. B 57 (2005) 63.
[39] M.H. Matloob, M.W. Roberts, J. Chem. Soc., Faraday Trans. 73 (1977) 1393.
[40] D.W. Johnson, M.H. Matloob, M.W. Roberts, J. Chem. Soc., Faraday Trans. 75 (1979) 2143.
[41] S.K. So, R. Franchy, W. Ho, J. Chem. Phys. 95 (1991) 1385.
[42] P. Dumas, M. Suhren, Y.J. Chabal, C.J. Hirschmugl, G.P. Williams, Surf. Sci. 371 (1997) 200.
[43] M. Iwamoto, S. Yokoo, K. Sakai, S. Kagawa, J. Chem. Soc., Faraday Trans. I 77 (1981) 1629.
[44] W.K. Hall, Y. Li, J. Catal. 129 (1991) 202.
[45] S.C. Chou, C.T. Yeh, T.H. Chang, J. Phys. Chem. B 101 (1997) 5828.
[46] J.A. Anderson, C.H. Rochester, Z.J. Wang, J. Mol. Catal. A 139 (1999) 285.
[47] B. Coq, R. Dutartre, F. Figueras, A. Rouco, J. Phys. Chem. 93 (1989) 4904.
[48] A. Guerrero-Ruiz, B. Bachiller-Baeza, P. Ferreira-Aparicio, I. Rodríguez-Ramos, J. Catal. 171 (1997) 374.
[49] M. Fernández-García, A. Martínez-Arias, I. Rodríguez-Ramos, P. Ferreira-Aparicio, A. Guerrero-Ruiz, Langmuir 15 (1999) 5295.
[50] P. Reyes, G. Pecchi, J.L.G. Fierro, Langmuir 17 (2001) 522.
[51] S. González, C. Sousa, M. Fernández-García, V. Bertin, F. Illas, J. Phys. Chem. B 106 (2002) 7839.
[52] J.A. Rodríguez, R.A. Campbell, D.W. Goodman, J. Phys. Chem. 94 (1990) 6936.
[53] S. González, C. Sousa, F. Illas, Surf. Sci. 531 (2003) 39.
[54] See instance http://www.webelements.com.
[55] T.B. Massalsiki, H. Okamoto, P.R. Subramanian, L. Kacprezak, Binary Alloy Phase Diagrams, second ed., ASM, Materials Parks, OH, 1992.
[56] J.P. Perdew, Y. Wang, Phys. Rev. B 45 (1992) 13244.
[57] G. Kresse, D. Joubert, Phys. Rev. B 59 (1998) 1758.
[58] P.E. Blöchl, Phys. Rev. B 50 (1994) 17953.
[59] P.E. Blöchl, P. Margl, K. Schwarz, Ab initio molecular dynamics with the projector augmented wave method, in Chemical Application of Density-Functional Theory, Am. Chem. Soc., USA, 1996.
[60] G. Kresse, J. Furthmüller, Phys. Rev. B 54 (1996) 11169.
[61] G. Kresse, J. Hafner, Phys. Rev. B 47 (1993) 558.
[62] G. Henkelman, H. Jonsson, J. Chem. Phys. 117 (2000) 303.
[63] G. Henkelman, H. Jonsson, J. Chem. Phys. 111 (1999) 7010.
[64] K.J. Laidler, Chemical Kinetics, third ed., Harper Collins, New York, 1987.
[65] S. Schewegmann, H. Over, V. De Renzi, G. Ertl, Surf. Sci. 375 (1997) 91.
[66] P.C. Wong, K.C. Hui, M.Y. Zhou, K.A.R. Mitchell, Surf. Sci. 165 (1986) L21.
[67] K.A. Peterlinz, S.J. Sibener, J. Phys. Chem. 99 (1995) 2817.
[68] M. Gierer, F. Mertens, H. Over, G. Ertl, R. Imbihl, Surf. Sci. 339 (1995) L903.
[69] D.N. Belton, C.L. DiMaggio, K.Y.S. Ng, J. Catal. 144 (1993) 273.
[70] D.T. Vu, K.A.R. Mitchell, Phys. Rev. B 49 (1994) 11515.
[71] Y. Xu, A.V. Ruban, M. Mavrikakis, J. Am. Chem. Soc. 126 (2004) 4717.